Available online at www.sciencedirect.com
SCIENCE DIRECT®
Planetary and Space Science 53 (2005) 1401–1418
Planetary and Space Science
www.elsevier.com/locate/pss

Response of peak electron densities in the martian ionosphere to day-to-day changes in solar flux due to solar rotation

Paul Withers*, Michael Mendillo

Center for Space Physics, Boston University, 725 Commonwealth Avenue, Boston, MA 02215, USA

Received 23 September 2004; received in revised form 27 July 2005; accepted 27 July 2005
Available online 27 October 2005

Abstract

Photochemical Chapman theory predicts that the square of peak electron density, N_m, in the dayside ionosphere of Mars is proportional to the cosine of solar zenith angle. We use Mars Global Surveyor Radio Science profiles of electron density to demonstrate that this relationship is generally satisfied and that positive or negative residuals between observed and predicted values of N_m^2 are caused by periods of relatively high or low solar flux, respectively.

Understanding the response of the martian ionosphere to changes in solar flux requires simultaneous observations of the martian ionosphere and of solar flux at Mars, but solar flux measurements are only available at Earth. Since the Sun's output varies both in time and with solar latitude and longitude, solar flux at Mars is not simply related to solar flux at Earth by an inverse-square law. We hypothesize that, when corrected for differing distances from the Sun, solar fluxes at Mars and Earth are identical when shifted in time by the interval necessary for the Sun to rotate through the Earth–Sun–Mars angle.

We perform four case studies that quantitatively compare time series of N_m at Mars to time series of solar flux at Earth and find that our hypothesis is satisfied in the three of them that used ionospheric data from the northern hemisphere. We define a solar flux proxy at Mars based upon the $E_{10.7}$ proxy for solar flux at Earth and use our best case study to derive an equation that relates N_m to this proxy. We discuss how the ionosphere of Mars can be used to infer the presence of solar active regions not facing the Earth.

Our fourth case study uses ionospheric observations from the southern hemisphere at latitudes where there are strong crustal magnetic anomalies. These profiles do not have Chapman-like shapes, unlike those of the other three case studies. We split this set of measurements into two subsets, corresponding to whether or not they were made at longitudes with strong crustal magnetic anomalies. Neither subset shows N_m responding to changes in solar flux in the manner that we observe in the three other case studies.

We find many similarities in ionospheric responses to short-term and long-term changes in solar flux for Venus, Earth, and Mars. We consider the implications of our results for different parametric equations that have been published describing this response.

Keywords: Mars; Ionosphere; Chapman theory; Solar flux; Magnetic fields

1. Introduction

1.1. Chemical composition of the martian atmosphere

The dominant constituent of the atmosphere of Mars is CO_2, which has a mixing ratio of over 95% in the lower atmosphere. A few percent of N_2 and variable, trace amounts of H_2O are also present (Owen, 1992). Chemical reactions involving these three species and sunlight produce other species, including CO, O, O_2, O_3, H, H_2, N, and NO. The noble gases are present, but chemically inert. Lighter species are enriched above the homopause, around 125 km altitude, due to diffusive separation (Barth et al., 1992).

1.2. Observations of the martian ionosphere

Present-day understanding of the martian ionosphere comes from the following observations: two vertical

*Corresponding author. Tel.: +1 617 353 1531; fax: +1 617 353 6463.
E-mail address: withers@bu.edu (P. Withers).

0032-0633/$ - see front matter © 2005 Elsevier Ltd. All rights reserved.
doi:10.1016/j.pss.2005.07.010

profiles of thermospheric composition from the Viking lander neutral mass spectrometers (Nier and McElroy, 1977); two vertical profiles of ionospheric composition from the Viking lander retarding potential analyzers (Hanson et al., 1977); ultraviolet spectroscopy of the airglow by Mariners 6, 7, and 9 (Barth et al., 1971, 1972; Stewart, 1972; Stewart et al., 1972); and many vertical profiles of electron density from many orbiters and flyby spacecraft (Kliore, 1992; Mendillo et al., 2003). Theoretical modelling of the martian ionosphere has benefitted greatly from the larger observational database at Venus, provided by the Pioneer Venus Orbiter, due to the many apparent similarities between the thermospheres and ionospheres of these two planets (Fox, 2004a; Shinagawa, 2004). However, many of these similarities have not yet been tested due to a lack of martian data. Major gaps in our current understanding could be filled by additional measurements of the neutral and ionized composition and of the dynamics of the thermosphere and ionosphere.

1.3. Ionospheric data from Mars Global Surveyor

Recent observations from the Mars Global Surveyor (MGS) spacecraft are improving our understanding of the martian ionosphere. Measurements by the MGS Radio Science (RS) instrument lead to vertical profiles of electron density as a function of altitude. Descriptions of the instrument and its data processing scheme have been published (Hinson et al., 1999, 2000; Tyler et al., 1992, 2001). Archived data can be downloaded from the Planetary Plasma Interactions (PPI) node of the Planetary Data System (PDS), online at http://pds-ppi.igpp.ucla.edu/, and from the RS team's website at http://nova.stanford.edu/projects/mgs/eds-public.html. Each vertical profile is accompanied in the archives by ancilliary information about the profile such as latitude, longitude, local solar time (LST), solar zenith angle (SZA), and measurement errors.

As of August, 2004, the MGS RS experiment team has so far released to the scientific community 2393 electron density profiles, which represents a significant increase in number over the 433 profiles measured prior to MGS (Mendillo et al., 2003). Due to constraints imposed by the observing geometry, these MGS measurements are restricted in latitude (60–85°N or °S) and SZA (70°–90°). It is challenging to obtain a global picture of the ionosphere from these observations. However, the sheer number of profiles and their extended timebase encourage other investigations focused on such effects as the martian seasons, interannual variability, and solar flux variations. The currently available data span December 1998–December 2002, over two martian years and over one-third of a solar cycle, although significant data gaps exist within this interval.

It is necessary for us to define some terminology to prevent possible confusion. A "day" is 24 h long, the rotation period of Earth. The rotation period of Mars is about 40 min longer than a day. If two measurements were made on the "same day", then they have the same UTC, Coordinated Universal Time, date. We use the UTC time zone because the times of the archived measurements are given in that time zone. Local solar time (LST) on Mars is measured in "hours" that are $\frac{1}{24}$ of a martian rotational period or "sol".

A typical electron density profile from MGS is shown in Fig. 1. Such profiles have a maximum, or peak electron density, near 140 km altitude, of $10^4-10^5\,\mathrm{cm}^{-3}$. We shall focus on this maximum, or primary peak, in this paper. Rishbeth and Mendillo (2004) suggested the label "M2" for this layer and "M1" for the weaker layer below it. Measurement uncertainties in electron density vary with altitude, but are on the order of a few thousand electrons cm^{-3}.

To date, MGS electron density profiles have been used to compare the martian and terrestrial ionospheric responses to changes in solar flux over a single 19 day period (Martinis et al., 2003; Mendillo et al., 2003, 2004; Rishbeth and Mendillo, 2004), to study the interaction between the ionosphere and the solar wind (Wang and Nielsen, 2003, 2004), to analyze the coupling between the thermosphere and the ionosphere (Bougher et al., 2001, 2004), to investigate the effects of X-rays on the ionosphere (Fox, 2004b), and to investigate the behavior of the ionosphere in regions of strong magnetic field (Krymskii et al., 2003, 2004; Breus et al., 2004, Withers et al., 2005).

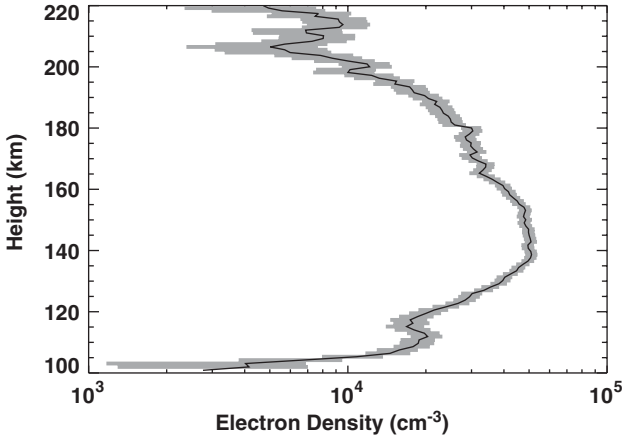

Fig. 1. Profile 0320A58A.EDS, a typical MGS RS electron density profile. It was measured at latitude 64.5°N, longitude 173.2°E, LST 2.8 h, Ls 76.3°, and solar zenith angle 85.1° on 15 November 2000 by the MGS RS instrument. The nominal profile is the solid line and 1σ uncertainties are marked by the shaded region. Note the disturbed topside, the primary peak (M2) at 140 km altitude, and the secondary feature (M1) at 110–120 km altitude.

1.4. Basic properties of the martian ionosphere and their causes

Detailed theoretical studies of the dayside martian ionosphere have been performed by many workers, including Chen et al. (1978), Shinagawa and Cravens (1989), Fox (1993), Fox et al. (1996), Shinagawa and Bougher (1999), and Krasnopolsky (2002). They show that electron densities in the vicinity of the primary peak, the "M2" layer in Rishbeth and Mendillo (2004), are well-described as an "alpha-Chapman layer" (Chapman, 1931a, b; Rishbeth and Garriott, 1969). The dominant ion production mechanism is photoionization of CO_2 to CO_2^+ by absorption of solar ultraviolet radiation, especially between 20 and 90 nm. Most photons with wavelengths shorter than 20 nm are absorbed below this primary peak and photons with wavelengths longer than 90 nm cannot ionize carbon dioxide. The atmospheric optical depth at these wavelengths is unity near the ionospheric peak, as expected (Martinis et al., 2003). CO_2^+ ions react rapidly with O to form O_2^+ ions, the dominant constituent of the ionosphere. The dominant ion loss mechanism is the dissociative recombination of O_2^+ ions with electrons to form O atoms, which are often suprathermal.

Above about 180 km, dynamical transport mechanisms begin to play an important role (Barth et al., 1992; Shinagawa, 2004). These mechanisms are not well understood in detail at the present time. Chen et al. (1978) and Fox (1993) had some success at reproducing observations using an ad hoc upward ion flow velocity of $\approx 1\,\mathrm{km\,s^{-1}}$. Shinagawa and Cravens (1989) and Shinagawa and Bougher (1999) suggested that horizontal gradients in magnetic pressure could cause ion transport comparable to that required.

Below the primary peak, many profiles show a less clear secondary peak, ledge, or shoulder near 110–120 km, which is due to (a) a maximum in direct photoionization by solar X-rays and (b) an increase in electron impact ionization, which is caused by energetic photoelectrons released when neutrals are ionized by the solar radiation (Fox et al., 1996). This so-called secondary ionization is more common for X-ray photons than it is for ultraviolet photons, so electron densities are increased when X-rays dominate photoionization, as they do near this secondary feature. Rishbeth and Mendillo (2004) suggested the label "M1" for this layer.

Other, less important, sources of ionization include meteor influx, charged particle influx, and non-solar sources of ultraviolet radiation and X-rays (Zhang et al., 1990; Fox et al., 1993; Kallio and Janhunen, 2001; Haider et al., 2002; Molina-Cuberos et al., 2003).

1.5. Aims and motivations

This paper has three aims. Our first is to examine how well the dependence of peak electron density on SZA, assuming constant solar flux, is modelled by simple Chapman theory, with a focus on whether residuals from a fit of observations to the model are related to changes in solar flux. Our second aim is to investigate how peak electron density responds to short-term changes in solar flux. Our third aim is to identify ionospheric responses to changes in solar flux that are due specifically to solar rotation.

The structure and variability of the martian ionosphere in the region of the "M1" and "M2" peak are dominated by photochemical processes, unlike the terrestrial F2 region, whose structure and variability are dominated by dynamical processes, such as transport of plasma by diffusion, electric fields, and neutral winds. The Sun–ionosphere connection is thus more direct for Mars than for the most strongly ionized region of the terrestrial ionosphere.

Ionospheres are a common phenomenon throughout the solar system and are probably present in extrasolar planets as well (Schunk and Nagy, 2000). Solar system ionospheres are all primarily driven by the same solar flux inputs. Their different responses are due to their different neutral compositions and vertical structures, distances from the Sun, and magnetic environments. By studying how the martian ionosphere responds to solar variability, and contrasting it with Earth and the other planets, we learn how these different local conditions affect the basic physical processes that govern the interaction of ions, neutrals, and radiation.

Understanding how the martian ionosphere responds to changes in solar flux will help us understand how the terrestrial ionosphere responds to changes in solar flux and separate those changes from those due to other causes, such as anthropogenic influences on the neutral atmosphere. It is also important for understanding what such ionospheric responses can tell us about the state and nature of our Sun. Finally, the martian ionosphere plays a major role in the escape of volatiles from Mars and has done so throughout solar system history. A better understanding of the ionosphere today will contribute to our understanding of the past habitability of Mars and the history of its water, despite seeming far-removed from these questions.

2. Dependence of dayside ionospheric electron density on solar zenith angle and solar flux

As discussed in Section 1.4, the dayside ionosphere in the vicinity of the peak electron density is controlled by

photochemical processes. The dayside electron number density, $N(z)$, should be given by an alpha-Chapman function (Rishbeth and Garriott, 1969; Chamberlain and Hunten, 1987):

$$\alpha N^2(z) = \frac{F_{1\,\mathrm{AU}}}{(D/1\,\mathrm{AU})^2}\frac{1}{Ch(X,\chi)}\frac{1}{He} \times \exp\left(1-\frac{z-z_m}{H}-\exp\left(-\frac{z-z_m}{H}\right)\right), \quad (1)$$

where α is the dissociative recombination rate of O_2^+, $1.95\times10^{-7}\,\mathrm{cm^3\,s^{-1}}$ for typical martian electron temperatures of 300 K (Schunk and Nagy, 2000), N is the number density of electrons, typically on the order of $10^4-10^5\,\mathrm{cm^{-3}}$, F is the flux of ionizing radiation at the top of the martian atmosphere, $F_{1\,\mathrm{AU}}$ is F normalized by an inverse-square law to a distance of 1 AU from the Sun, typically $10^{10}-10^{11}$ photons $\mathrm{cm^{-2}\,s^{-1}}$ (Tobiska et al., 2000; Tobiska, 2001; Martinis et al., 2003), D is the actual Mars–Sun distance, typically 1.5 AU, Ch is a dimensionless geometrical correction factor, which reduces to $\sec(\chi)$ for sufficiently small values of χ (Smith and Smith, 1972), χ is the SZA, typically 80° for the MGS RS data, H is the constant scale height of the neutral atmosphere, typically 12 km, e, the base of the natural logarithm, is 2.71828..., z is altitude, typically 100–200 km, z_0 is a reference altitude, defined to be the altitude at which N is maximized for $Ch=1$ and typically ~120 km, $z_m = z_0 + H\ln Ch$, and X is the dimensionless ratio $(z+R)/H$, where R is the planetary radius, 3400 km. z_0 does not depend on Ch, but z_m, the altitude at which N is maximized, does (Rishbeth and Garriott, 1969). Ch is only weakly dependent on H and z for the martian ionosphere and representative values, such as $H=12$ km and $z=150$ km, can be used in the formulae of Smith and Smith (1972) without significant error. Chamberlain and Hunten (1987) discuss the assumptions implicit in Eq. (1).

Eq. (1) is only strictly correct for ionization produced by monochromatic radiation, whereas the martian ionosphere is produced by photons with wavelengths below 90 nm, generally in the UV and X-ray portions of the spectrum. Martinis et al. (2003) show a solar flux spectrum and subsequent photoionization rate at Mars as a function of wavelength. Almost all of the ionization in the vicinity of the peak electron density is caused by wavelengths that have optical depths of unity at the same altitude. Since flux at any wavelength within this range is absorbed equally by any given length of atmospheric column on Mars, it is reasonable to apply monochromatic Chapman theory to the formation of the ionospheric peak in the martian atmosphere despite the actual range of ionizing wavelengths.

Eq. (1) can be manipulated to show that the peak electron density, N_m, satisfies (Rishbeth and Garriott, 1969; Chamberlain and Hunten, 1987):

$$N_m^2(D/1\,\mathrm{AU})^2 H = \frac{1}{Ch(X,\chi)}\frac{F_{1\,\mathrm{AU}}}{\alpha e}. \quad (2)$$

We define P as $N_m^2(D/1\,\mathrm{AU})^2H$.

2.1. Testing predictions of ionospheric dependence on solar zenith angle

Previous workers have shown that Eq. (2) describes the dependence of N_m on Ch or, equivalently, χ when $F_{1\,\mathrm{AU}}$ is constant (Barth et al., 1992). We shall extend their studies with MGS RS data and investigate whether the assumption of constant $F_{1\,\mathrm{AU}}$ affects the results.

On the right-hand side of Eq. (2), $1/Ch$ is known to a high degree of accuracy from the geometry of the MGS RS observations. All of the quantities on the left-hand side of Eq. (2) can be deduced from vertical profiles of electron density, $N(z)$. H, the neutral atmospheric scale height, can be found by fitting the observed dependence of electron density on altitude to the exponential altitude dependence of Eq. (1), or to an approximation of this altitude dependence. There are a number of different ways to perform such a fit. We first consider the form

$$N^2 = N_m^2\exp(1-x-\exp(-x)). \quad (3)$$

A non-linear least squares fit to Eq. (3), where $x=(z-z_m)/H$ and N_m, z_m, and H are unknowns, offers a solution for H with uncertainties, but is relatively challenging to implement and slow to converge on a solution (Press et al., 1992). For sufficiently small x, the exponential expression in Eq. (3) can be expanded as a power series as shown in Eq. (4), where $a_0 = N_m(1-z_m^2/4H^2)$, $b_0 = N_m z_m/2H^2$, and $c_0 = -N_m/4H^2$ (Breus et al., 2004):

$$N(z) = a_0 + b_0 z + c_0 z^2. \quad (4)$$

This approach offers a fast and standard solution technique, and gives uncertainties on a_0, b_0, and c_0, but not on the desired H (Bevington, 1969). For sufficiently small x, the exponential expression in Eq. (3) can also be expanded as shown in Eq. (5), where $a_1 = \ln N_m - z_m^2/4H^2$, $b_1 = z_m/2H^2$, and $c_1 = -1/4H^2$:

$$\ln N = a_1 + b_1 z + c_1 z^2. \quad (5)$$

Since c_1 is solely a function of H and does not depend on N_m or z_m, uncertainties on H can be obtained from those on c_1. We use fits to Eq. (5) to derive H in this paper. Choosing an appropriate vertical range for the fit is also important. The accuracy of the power series expansion is not symmetrical with altitude about z_m. It is accurate to better than 10% for $-0.5<x<1.0$ and we use this range for our fit. To determine whether a data point falls within this range, we assume that z_m equals the altitude at which $N(z)$ is maximized, without

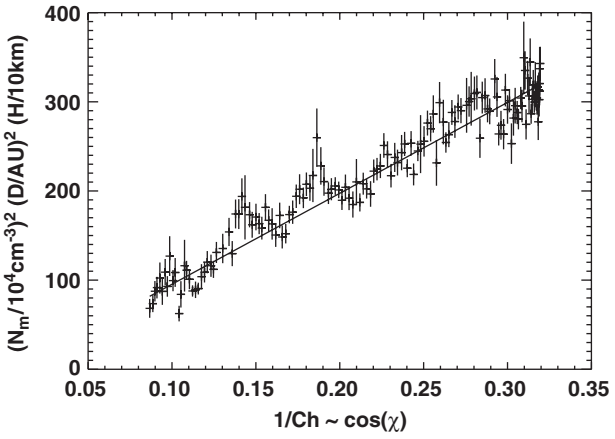

Fig. 2. Daily average values of $N_m^2 D^2 H$ versus $1/Ch$ from November 2000 to March 2001. At the start of November 2000, Ls = 70.2°, LST = 2.8 h, latitude = 63.4°N, $\chi = 86.6°$, and $1/Ch = 0.09$. These properties changed monotonically until the end of March 2001, when their values were: Ls = 136.4°, LST = 7.0 h, latitude = 85.4°N, $\chi = 71.8°$, and $1/Ch = 0.32$. Vertical lines on each data point show the $\pm 1\sigma$ uncertainty in each day's average value of $N_m^2 D^2 H$. Horizontal lines on each data point merely mark the nominal value of each data point; their length has no significance since the range in $1/Ch$ during any given day is very small.

consideration of the measurement errors in $N(z)$, and that $H = 10$ km. We find that H is typically 12 km and σ_H is typically 3 km.

A large range in $1/Ch$ is desired in order to test the dependence of peak electron density on SZA predicted by Eq. (2). Accordingly, we select MGS RS data from November 2000 ($\chi = 86.6°$ and $1/Ch = 0.09$) to March 2001 ($\chi = 71.8°$ and $1/Ch = 0.32$), which spans nearly the full range of χ in the entire dataset and has continuous data coverage. We plot P against $1/Ch$ in Fig. 2. To reduce the clutter in the figure, we averaged values of P and $1/Ch$ for each day during the period. A typical day had seven profiles. This also reduces the effect of any variations with longitude that might be present.

We anticipate that the data should fall on a straight line with gradient $F_{1\,\mathrm{AU}}/\alpha e$ and intercept at the origin. The best fit in Fig. 2 is

$$(N_m/10^4\,\mathrm{cm}^{-3})^2 (D/1\,\mathrm{AU})^2 (H/10\,\mathrm{km}) = (-6.6 \pm 3.3) + (1020 \pm 20) \times 1/Ch. \quad (6)$$

The intercept is quite close to the anticipated value of zero. Closer examination of the residuals reveals that they are not randomly distributed with respect to $1/Ch$ or, equivalently, time. Groups of positive residuals are clustered together, as are negative residuals, and this will be examined further in Section 3.3.

2.2. Derived value of $F_{1\,\mathrm{AU}}$

Comparing Eqs. (2) and (6) shows that $F_{1\,\mathrm{AU}}/\alpha e = (10.2 \pm 0.2) \times 10^{16}\,\mathrm{cm}^{-5}$. The recombination coefficient, α, equals $2 \times 10^{-7}\,\mathrm{cm}^3\,\mathrm{s}^{-1}$ for electron temperatures around 300 K and e is 2.71828... (Fox et al., 1996; Schunk and Nagy, 2000). Hence $F_{1\,\mathrm{AU}} = (5.5 \pm 0.1) \times 10^{10}\,\mathrm{cm}^{-2}\,\mathrm{s}^{-1}$. There were no direct measurements of solar flux at Mars during this period. However, solar flux has been measured at Earth by a variety of instruments for many years. These measurements have been incorporated into the publicly available Solar2000 model (Tobiska et al., 2000; Tobiska, 2001). This model yields a flux of $\approx 4 \times 10^{10}$ photons $\mathrm{cm}^{-2}\,\mathrm{s}^{-1}$ at Earth during this period for wavelengths between 20 and 90 nm, which is reasonably consistent with our value of $F_{1\,\mathrm{AU}}$. This agreement confirms that Eq. (2) is quite accurate.

2.3. $F_{10.7}$, $E_{10.7}$, and solar flux proxies

The flux emitted from a region of the Sun varies with time and position on the solar disk. Away from the Sun, solar flux varies radially according to the inverse square of distance from the Sun. Since Mars only faces the same hemisphere of the Sun as Earth during infrequent oppositions (when Mars is anti-sunward of Earth along the Earth–Sun line), and its orbit is more elliptical than Earth's, there is a need to specify quantitatively how characterizations of solar flux at Earth can be applied to Mars.

We wish to use a single number, not a range of wavelengths, to characterize solar flux. We shall move beyond our qualitatively defined $F_{1\,\mathrm{AU}}$ to a more quantitative solar flux proxy. Studies of the terrestrial ionosphere have long used the $F_{10.7}$ index, a measure of solar flux at non-ionizing radio wavelengths (2800 MHz) that correlates reasonably well with fluxes at ionizing UV wavelengths, but not equally well at all timescales. This index, generally quoted in "radio flux units", has also been used to describe the response of other planetary ionospheres to changes in solar flux over a solar cycle. Since the $F_{10.7}$ index is not a direct measure of ionizing radiation, a new proxy has recently been introduced—$E_{10.7}$ (Tobiska et al., 2000; Tobiska, 2001). Since this proxy is used frequently in this paper, we shall describe the rationale behind its development and its definition.

Tobiska et al. (2000) wished to find a proxy that represented the volume averaged heating rate, $Q(t)$, which has units of $\mathrm{J\,m}^{-3}\,\mathrm{s}^{-1}$, in the thermosphere of the *Earth* better than $F_{10.7}$. He examined the solar energy flux spectrum, $I(\lambda, t)$, which has units of $\mathrm{J\,m}^{-2}\,\mathrm{s}^{-1}\Delta\lambda^{-1}$ and found that $Q(t)$, derived from a one-dimensional, time-dependent thermospheric model, correlated well with the integrated value of $I(\lambda, t)$ between 1.862 and 104.9 nm, $E(t)$, which has units of $\mathrm{J\,m}^{-2}\,\mathrm{s}^{-1}$. $E(t)$ was derived from observations. In order to facilitate comparison between a new proxy and $F_{10.7}$, he then created a new proxy, $E_{10.7}$, based on a power

series in $E(t)$:

$$E_{10.7} = a_0 + a_1 E(t) + a_2 E(t)^2 + \cdots. \quad (7)$$

The coefficients, a_i, are defined (a) to give $E_{10.7}$ the same units and approximate magnitudes as $F_{10.7}$ and (b) to maximize the correlation between $F_{10.7}$ and $E_{10.7}$. Since $E_{10.7}$ is not a direct observable, historical values may change as its generating function, Eq. (7), evolves. This proxy is only defined at the Earth, whereas we need a solar flux proxy applicable at Mars, so we shall now extend the definition of $E_{10.7}$.

The solar flux (units of $\mathrm{J\,m^{-2}\,s^{-1}\Delta\lambda^{-1}}$) at any location in the solar system, any wavelength, and any time can be specified as $I(r,\theta,\phi,\lambda,t)$ where r,θ,ϕ are position coordinates. We define $E(r,\theta,\phi,t)$ as follows:

$$E(r,\theta,\phi,t) = \int_{\lambda_1}^{\lambda_2} I(r,\theta,\phi,\lambda,t)\,\mathrm{d}\lambda, \quad (8)$$

where λ_1 is 1.862 nm and λ_2 is 104.9 nm. We define $E_{10.7}(r,\theta,\phi,t)$ as a function of $E(r,\theta,\phi,t)$ as in Eq. (7), using coefficients appropriate to version 2.23 of the Solar2000 model (Tobiska et al., 2000; Tobiska, 2001). We will use two specific examples of this general proxy: $E_{10.7}^{\mathrm{Earth,1\,AU}}$ and $E_{10.7}^{\mathrm{Mars,1\,AU}}$. These are functions of time, though we find it convenient to omit the explicit dependence from these symbols. $E_{10.7}^{\mathrm{Earth,1\,AU}}$ is calculated at the heliocentric latitude and longitude of Earth and a distance of 1 AU from the Sun. Similarly, $E_{10.7}^{\mathrm{Mars,1\,AU}}$ is calculated at the heliocentric latitude and longitude of Mars and a distance of 1 AU from the Sun. Since solar flux is proportional to the inverse square of distance from the Sun, any use of this proxy to represent the actual flux incident on the top of the martian atmosphere will have to include this weighting factor. Note that the orbits of Earth and Mars are almost coplanar. We obtain daily values of $E_{10.7}^{\mathrm{Earth,1\,AU}}$ from the publicly available Solar2000 model (Tobiska et al., 2000; Tobiska, 2001). This model incorporates a wide variety of measurements to generate historical solar fluxes. We use version 2.23 of this model, with the S2K/ASTM490 model selected, throughout this paper. Other versions will give similar, but not identical, results due to the continued improvement of the model using new and old datasets (Tobiska and Bouwer, 2004). There are no measurements of solar flux at Mars and we shall discuss how to obtain $E_{10.7}^{\mathrm{Mars,1\,AU}}$ later in Section 3.1. We will occasionally use similar superscripts on $F_{10.7}$ for emphasis when we discuss comparisons to other work.

3. Ionospheric response to short-term changes in solar flux

Having established in Section 2.1 that ionospheric peak electron densities are not satisfactorily described by a model with constant solar flux, we wish to study how the ionosphere responds to short-term changes in solar flux. Since $E_{10.7}^{\mathrm{Mars,1\,AU}}$ should be proportional to $F_{1\,\mathrm{AU}}$, we can manipulate Eq. (2) to obtain

$$N_m(D/1\,\mathrm{AU})\sqrt{H\,Ch} \propto \sqrt{\frac{E_{10.7}^{\mathrm{Mars,1\,AU}}}{\alpha}}. \quad (9)$$

The O_2^+ recombination coefficient, α, is a complicating factor in Eq. (9). For electron temperatures, T_e, below 1200 K, it depends on T_e as follows: $\alpha = 1.95\times10^{-7}\times(300\,\mathrm{K}/T_e)^{0.7}\,\mathrm{cm^3\,s^{-1}}$ (Schunk and Nagy, 2000). Electron temperature may vary with solar flux and SZA. Existing observations are not sufficient to permit calculation of T_e given only solar flux and SZA (Rishbeth and Garriott, 1969; Fox et al., 1996).

Thus a plot of $N_m(D/1\,\mathrm{AU})\sqrt{H\,Ch}$ versus $\sqrt{E_{10.7}^{\mathrm{Mars,1\,AU}}}$ may not be the straight line through the origin suggested by a simple interpretation of Eq. (9). Since we will only compare ionospheric measurements made within a narrow range of SZA, we do not expect large changes in T_e due to variations in SZA. We assume that changes in T_e are similar to changes in neutral temperatures and note that thermospheric general circulation models only predict a 50% increases in neutral temperatures at ionospheric altitudes from solar minimum to maximum (Bougher et al., 1990). A 50% variation in T_e over a full solar cycle causes only a 15% change in N_m. Since this dependence is so weak, we will follow the example of other workers and deal with the problem of unknown electron temperatures by parameterization (Hantsch and Bauer, 1990; Breus et al., 2004). As long as electron temperature has a monotonic dependence on $E_{10.7}^{\mathrm{Mars,1\,AU}}$, we can write

$$N_m(D/1\,\mathrm{AU})\sqrt{H\,Ch} \propto (E_{10.7}^{\mathrm{Mars,1\,AU}})^m. \quad (10)$$

We define Q as $N_m(D/1\,\mathrm{AU})\sqrt{H\,Ch}$. In the limit of fixed electron temperature, m should be one-half. If electron temperature increases as solar flux increases, then m should be greater than one-half.

3.1. Variation of $E_{10.7}^{\mathrm{Earth,1\,AU}}$ with time

Fig. 3 shows how $E_{10.7}^{\mathrm{Earth,1\,AU}}$ varies during 1998–2001. Solar2000 generates values of $E_{10.7}^{\mathrm{Earth,1\,AU}}$ once per day (at UTC noon) without any error bars, although the actual solar flux can and does vary on shorter timescales.

A secular increase due to the 11 year solar cycle can be seen in Fig. 3. The preceding solar minimum was in 1996 and the (unusually broad) solar maximum occurred in 2000–2002. Superimposed on this trend is an oscillation with a ~27 day period. However, many additional features are also present. The variation in $E_{10.7}^{\mathrm{Earth,1\,AU}}$ with time is more complicated than merely a secular trend plus a sinusoidal variation with a 27 day period.

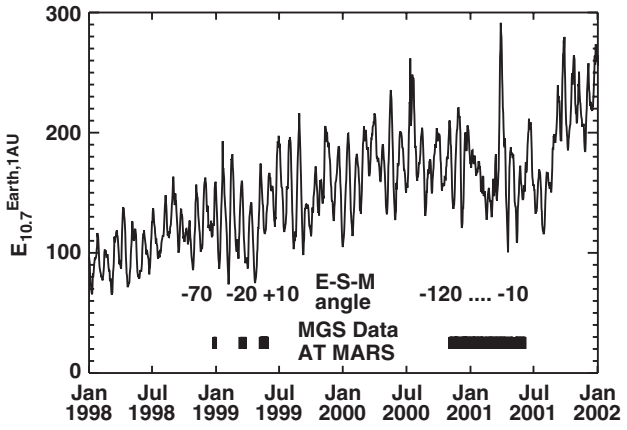

Fig. 3. $E_{10.7}^{\text{Earth,1 AU}}$ during 1998–2001. Intervals during which MGS RS ionospheric data are available are marked by thick solid bars (December 1998, March 1999, May 1999, and November 2000–June 2001). Above those bars, the Earth–Sun–Mars (E–S–M) angle for that time is shown in degrees. Oppositions occur when the E–S–M angle is zero, so data are available just before and just after the 1999 opposition, and just before the 2001 opposition.

Solar flux varies with solar latitude and longitude as well as time. Regions that contribute strongly to the total ultraviolet flux from the Sun are called "active regions". The characteristic timescale for change in solar flux from a given region on the Sun is greater than the solar rotation period, so observed periodicities in solar flux are related to the solar rotation period, not to the timescale for temporal changes in an active region. The solar rotation period varies with latitude, being shortest (25.4 days) at the equator. Since solar flux at Earth (and Mars) is dominated by photons from the equatorial region of the Sun, the periodicity of solar flux observed at Earth is due to the combination of the rotation of the equatorial region of the Sun and the revolution of the Earth about the Sun with a 365.25 day period (Hargreaves, 1992). A 27 day periodicity seen at Earth corresponds to a 26 day periodicity at Mars due to the difference in their orbital periods, but we shall ignore this small difference in our work.

3.2. Relation of $E_{10.7}^{\text{Earth,1 AU}}$ and $E_{10.7}^{\text{Mars,1 AU}}$

We are still left with the problem of relating the unknown $E_{10.7}^{\text{Mars,1 AU}}$ to the known $E_{10.7}^{\text{Earth,1 AU}}$ for any orbital configuration. Temporal and spatial variations in the Sun's output are seen by the ionospheres of Earth and Mars as temporal variations only, which makes it challenging to use one to derive the other. There are two cases in which $E_{10.7}^{\text{Earth,1 AU}}$ can plausibly be used to derive $E_{10.7}^{\text{Mars,1 AU}}$. The first is trivial: when Mars is at opposition, $E_{10.7}^{\text{Earth,1 AU}}$ and $E_{10.7}^{\text{Mars,1 AU}}$ are identical because both planets are at the same heliocentric latitude and longitude. Recall that their (different) distances from the Sun are not used in our definition of these solar flux proxies.

The second case requires that $E_{10.7}^{\text{Earth,1 AU}}$ be very similar from one solar rotation to the next. When this criterion is satisfied, $E_{10.7}^{\text{Earth,1 AU}}$ can be equated to $E_{10.7}^{\text{Mars,1 AU}}$ if $E_{10.7}^{\text{Earth,1 AU}}$ is shifted in time by the length of time necessary for the Earth-facing hemisphere of the Sun to rotate to face Mars. This operation requires knowledge of the solar rotation period and the Earth–Sun–Mars angle, which can be obtained from the orbital positions of Earth and Mars. We adopt the convention that Earth–Sun–Mars angles are negative prior to opposition, when Earth is trailing Mars, and positive after opposition, when Mars is trailing Earth.

3.3. Fit residuals

The residuals from Fig. 2 are plotted versus $1/Ch$ in Fig. 4. Values of $1/Ch$ for the MGS RS observations are a monotonically increasing function of time between November 2000 and March 2001. $E_{10.7}^{\text{Earth,1 AU}}$ is a function of time, but it can be expressed as a function of $1/Ch$ using this monotonic relationship. It is plotted as such in Fig. 4. Some peaks and troughs in both data series are marked with vertical lines.

If one data series were shifted in time by ~8 days, then the two sets of vertical lines would match up together. Is this 8 day interval the time required for the Sun to rotate from facing one planet to facing the other? Fig. 5 shows the orbital positions of Earth and Mars for this period. The Earth–Sun–Mars angle was -116° at the start of November 2000, when $1/Ch$ was 0.09. The

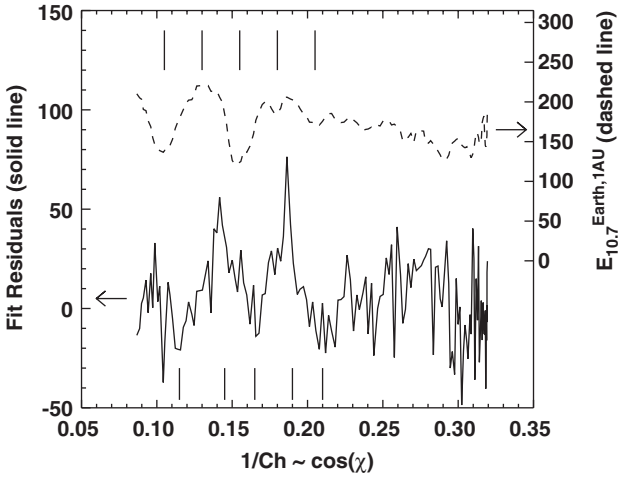

Fig. 4. The solid line shows the residuals from the fit in Fig. 2, in the same units. It uses the scale on the left-hand axis. Error bars on the residuals are not shown, since the purpose of this figure is to make a qualitative, not quantitative, comparison. The error bars on the observations, shown in Fig. 2, have a mean value of 16 in these units. $1/Ch$ is a monotonically increasing function of time between November 2000 and March 2001, so time series of other data can be plotted against it. The dashed line shows $E_{10.7}^{\text{Earth,1 AU}}$, a time series, plotted against $1/Ch$. It uses the scale on the right-hand axis. Some peaks and troughs in both data series are marked with vertical lines and discussed in the text. The vertical lines are about 14 days apart.

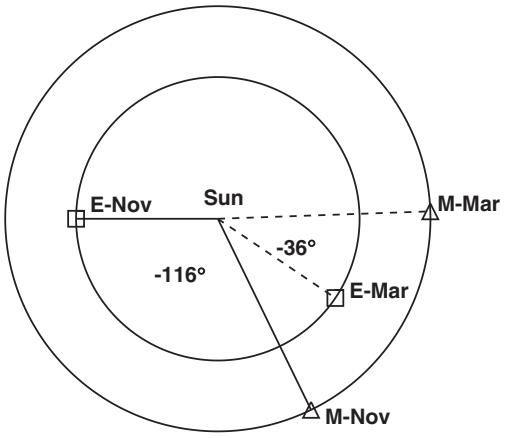

Fig. 5. The orbital positions of Earth (E) and Mars (M) are shown for early November 2000 (Nov) and late March 2001 (Mar), corresponding to the period shown in Figs. 2 and 4. The orbit of Mars is depicted as circular with a radius of 1.5 AU for simplicity. Solid lines radiating from the Sun show the Earth–Sun–Mars angle of -116° at the start of this period and similar dashed lines show the Earth–Sun–Mars angle of -36° at the end of this period.

Earth–Sun–Mars angle monotonically decreased to -82° by the end of December 2000, when $1/Ch$ was 0.20. These positions correspond to timeshifts of 9 and 6 days, respectively, so there is good qualitative agreement. This gives us confidence that the martian ionosphere sometimes responds to solar flux as measured at Earth with a lag/lead time set by the solar rotation period and Earth–Sun–Mars angle, but the idea needs testing more quantitatively.

3.4. Hypotheses to be tested

We have two related hypotheses that can be investigated concerning the response of the martian ionosphere to short-term changes in solar flux. The first is that the martian ionosphere satisfies Eq. (10) on day-to-day timescales for some value of m. The second is that $E_{10.7}^{\text{Mars,1 AU}}$ is a useful proxy for solar flux, in terms of its effects on the martian ionosphere, when $E_{10.7}^{\text{Mars,1 AU}}$ is derived from $E_{10.7}^{\text{Earth,1 AU}}$ using the timeshift method we have outlined above. Other workers have fitted Eq. (10) to observations with year-to-year changes in solar flux and determined a best fit value of m (Hantsch and Bauer, 1990; Breus et al., 2004). A typical result for m is 0.36. For the moment, we shall take it as proven that Eq. (10) is satisfied for some value of m. We return to this subject in Section 4.5. We shall focus, therefore, on testing whether $E_{10.7}^{\text{Earth,1 AU}}$ can be related to $E_{10.7}^{\text{Mars,1 AU}}$ by the timeshift method.

MGS RS data, as shown at the bottom of Fig. 3, are only available for restricted periods during its mission. We have selected four periods for further study. Two of them are near opposition, providing "control" samples. The other two are not, but occur when $E_{10.7}^{\text{Earth,1 AU}}$ is very similar from one solar rotation to the next. The periods are about 20–25 days long because it seems reasonable that their length should be comparable to the solar rotation period.

3.5. Method

1. Define period of interest, of duration approximately equal to one solar rotation.
2. Calculate daily average of Q, Eq. (10), and error bar for each UTC day during this period.
3. Obtain $\sqrt{E_{10.7}^{\text{Earth,1 AU}}}$ for each UTC day in this period.
4. Calculate the correlation coefficient between these two data series (Bevington, 1969).
5. Obtain a new $\sqrt{E_{10.7}^{\text{Earth,1 AU}}}$ series using a period offset forwards or backwards in time by an integer number of UTC days from the original period.
6. Calculate the new correlation coefficient and repeat for offsets of $-28, -27, \ldots, 28$, days. This range is chosen to capture at least one full solar rotation. Negative offsets should occur prior to opposition, when Earth is trailing Mars, and positive offsets should occur after opposition, when Mars is trailing Earth.
7. Examine the correlation coefficient as a function of the applied offset, which we will call the "correlation curve".

3.6. Anticipated behavior

Suppose $\sqrt{E_{10.7}^{\text{Earth,1 AU}}} = a + b\sin(2\pi t/T - \gamma)$ and, following Eq. (10), $Q = (f + g\sin(2\pi t/T))^m$. a and f are mean values, b and g are the amplitudes of the modulation induced by solar rotation, t is time, T is effectively the solar rotation period, γ is the Earth–Sun–Mars angle, and m is an exponent. We have neglected the minor difference, $\sim$1 day, in T as seen from Earth and Mars. If mg/f is sufficiently small, then $Q = f^m + mgf^{m-1}\sin(2\pi t/T)$. In this case, the ratio of the sinusoidal amplitude of Q to the mean is mg/f. If we apply an offset, t_{off}, to the $\sqrt{E_{10.7}^{\text{Earth,1 AU}}}$ data series then it becomes $a + b\sin(2\pi t/T + 2\pi t_{\text{off}}/T - \gamma)$. The correlation coefficient between this offset data series and the Q data series is $\cos(2\pi t_{\text{off}}/T - \gamma)$. This is a function of t_{off}. This "correlation curve" has a maximum when $2\pi t_{\text{off}}/T = \gamma$ and is independent of m.

If one data series is modified by the addition of a *small* normally distributed error term, then the correlation curve becomes $\cos(2\pi t_{\text{off}}/T - \gamma) \times \varepsilon$, where ε is less than unity. If the correlation curve is more-or-less sinusoidal with a given period, then the two data series must both be more-or-less sinusoidal with the *same* period.

The following conclusions may be drawn if the correlation curve for any of the periods is more-or-less sinusoidal: (a) its sinusoidal shape requires that both data series are approximately sinusodial with the same period, (b) its phase fixes the phase difference between $E_{10.7}^{\text{Earth,1 AU}}$ and $E_{10.7}^{\text{Mars,1 AU}}$, and (c) small deviations of its amplitude from unity imply small deviations in the data from our two hypotheses. The period of the correlation should be that of the ~27 day period in $E_{10.7}^{\text{Earth,1 AU}}$. The phase of the correlation should correspond to the observed Earth–Sun–Mars angle.

4. Results

4.1. Results from Periods 1–3

Table 1 details the four periods we examined and the results, and Fig. 6 shows the results for Periods 1–3 only. Each row of panels corresponds to one period. Period 4 is discussed in Section 4.3. Periods are not listed in chronological order for reasons that will be discussed below.

The shape of the correlation curves on the right-side of Fig. 6 for each of Periods 1–3 are approximately sinusoidal, peak–peak and trough–trough spacings are consistent with those in the corresponding $E_{10.7}^{\text{Earth,1 AU}}$ data, the amplitudes of peaks and troughs are similar to each other, and the observed offsets of maximum correlation (see Table 1) are consistent with the predicted offsets. Periods 1 and 2 were selected for their repeatable $E_{10.7}^{\text{Earth,1 AU}}$. Period 3 is near opposition. The magnitude of maximum correlation decreases from Period 1 to Period 2, and from Period 2 to Period 3.

Results for Periods 1–3 are as predicted in Section 3.6, where it was assumed that mg/f was small. Recall that the ratio of the sinusoidal amplitude of Q to the mean is mg/f. Referring to the left column of Fig. 6, the peak-to-peak amplitude of Q is about 6 and the mean is about 30. Thus $mg/f \approx 0.09$, which is small enough for Section 3.6 to be valid.

Mendillo et al. (2003) examined MGS RS data from a fifth period, 9–27 March, 1999, when the Earth–Sun–Mars angle was $\approx -20°$, which corresponds to a nominal offset of −1.5 days. They found that N_m^2 was approximately proportional to $E_{10.7}^{\text{Mars,1 AU}}$ when they assumed a zero day offset, but they did not examine how this relationship changed with different offsets.

Some features in Fig. 6 can be matched to corresponding features in Fig. 4. The peak in $E_{10.7}^{\text{Earth,1 AU}}$ at $1/Ch \approx 0.31$ in Fig. 4 can be seen around 15 March 2001 in panel (a) of Fig. 6. The trough in $E_{10.7}^{\text{Earth,1 AU}}$ at $1/Ch \approx 0.10$ in Fig. 4 can be seen around 15 November 2000 in panel (c) of Fig. 6, and subsequent peaks and troughs can also be matched between the two Figures.

Finally, Table 1 shows that the magnitudes of maximum correlation for Periods 1–3 increase as the mean value of $E_{10.7}^{\text{Mars,1 AU}}$ increases *and* as the range in $E_{10.7}^{\text{Mars,1 AU}}$ during the Period increases. The mean value of $E_{10.7}^{\text{Mars}}$ increases as the range in $E_{10.7}^{\text{Mars,1 AU}}$ increases for all of these three Periods, so they cannot be separated as possible physical causes of changes in magnitudes of maximum correlation. Either one, or the other, or both of these possible causes seems physically reasonable. We have ordered Periods 1–3 so that the magnitude of maximum correlation decreases from Period 1 to Period 3.

4.2. Solar flux proxy validation

Correlations are not improved by using a different solar flux proxy. We tested this timeshift method with

Table 1
Periods studied

Period	1	2	3	4
Start date	30 March 2001	5 November 2000	10 May 2001	6 May 1999
End date	19 April 2001	25 November 2000	6 June 2001	29 May 1999
Number of profiles	140	178	208	220
Range in χ (deg)	71.8–72.8	83.8–86.2	76.0–87.0	78.5–86.9
Range in latitude (°N)	83.4–85.4	63.7–65.7	69.0–80.1	−69.1 to −64.6
Range in LST (h)	7.4–8.8	2.8–2.8	6.1–8.2	12.0–12.2
Range in Ls (deg)	138.0–148.2	72.0–81.0	158.9–173.8	134.7–146.3
Range in ESM[a] angle (deg)	−34 to −24	−114 to −103	−14 to −3	5–16
Predicted offset of MC[b] (days)	−3 to −2	−9 to −8	−1 to 0	0 to +1
Observed offset of MC[b] (days)	−4 to +3	−9 to −1	−7 to +4	N/A
Range[c] in $E_{10.7}^{\text{Mars,1 AU}}$	117–291	137–210	109–173	116–174
Magnitude of MC[b]	0.82 ± 0.05	0.42 ± 0.13	0.14 ± 0.12	N/A
Reason for selecting period	RE[d]	RE[d]	NO[e]	NO[e]
Typical sub-solar latitude (°N)	15	25	6	15

[a]Earth–Sun–Mars.
[b]Maximum correlation.
[c]Range in $E_{10.7}^{\text{Mars,1 AU}}$ during each Period is calculated using $E_{10.7}^{\text{Earth,1 AU}}$ and the predicted offset.
[d]Repeatable $E_{10.7}^{\text{Earth,1 AU}}$.
[e]Near opposition.

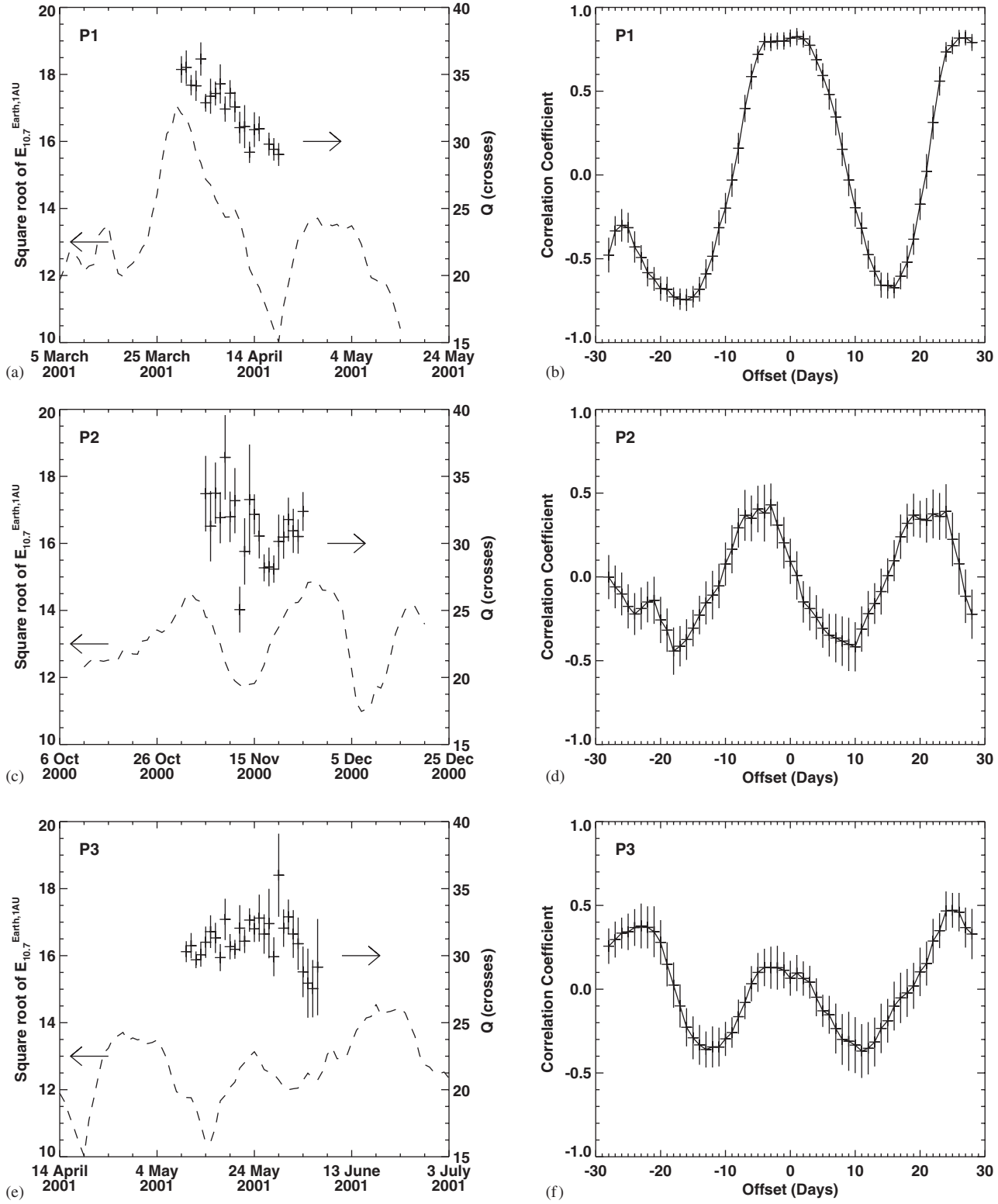

Fig. 6. Each row displays results from one Period, going from Period 1 at the top to Period 3 at the bottom. The left panel in each row shows daily averages of $Q = N_m/(10^4\,\mathrm{cm}^{-3})\sqrt{H/(10\,\mathrm{km})}Ch(D/\mathrm{AU})$ as measured at Mars for each day in the Period (crosses, with the height of the cross corresponding to the $\pm 1\sigma$ error bar, with scale on the right-hand axis) and $\sqrt{E_{10.7}^{\mathrm{Earth,1\,AU}}}$ (dashed line with scale on the left-hand axis) from 28 days before the start of the Period to 28 days after the end of the Period. The longer series of $E_{10.7}^{\mathrm{Earth,1\,AU}}$ data is needed to compare the ionospheric observations with earlier or later solar fluxes. Horizontal arrows indicate the respective axes. The right panel in each row shows the correlation curve (crosses joined by solid line) of these two data series as a function of the offset between them. The height of each cross in the correlation curve corresponds to the $\pm 1\sigma$ error bar.

$E_{10.7}^{\text{Earth,1 AU}}$, $F_{10.7}^{\text{Earth,1 AU}}$, and the intensity of the He 30.38 nm line at Earth's heliocentric latitude and longitude and a distance of 1 AU from the Sun. All three of these candidate proxies were generated by Solar2000. The He 30.38 nm line is a major contributor to the total ionizing flux. The offsets of maximum correlation occurred closest to their predicted values for Periods 1–3 using $E_{10.7}$, slightly further away using the He 30.38 nm line, and significantly further away using $F_{10.7}$. Magnitudes of maximum correlation were quite similar for $E_{10.7}$ and the He 30.38 nm line. From an observational standpoint, measuring the solar flux in a single spectral line at Mars might be simpler than measuring a flux with spectral resolution over a range of wavelengths if a Mars-dedicated solar flux proxy is desired. Following the terrestrial ionospheric study of Richards (1994), we also used the 81-day averages of these three candidate proxies and the mean of their daily values and their 81-day averages. The 81-day averages are much too constant to correlate well with the observed large changes in peak electron density and we saw no improvement from averaging this long-term average with the daily value. We conclude that, despite being optimized to represent heating in the terrestrial thermosphere, $E_{10.7}$ is a useful proxy for solar flux in terms of its effects on the martian ionosphere.

4.3. Results from Period 4

Unlike Periods 1–3, many profiles from Period 4 are poorly fit by an alpha-Chapman function of the form in Eq. (1). Examples of this can be seen in Fig. 7. Scale heights derived from these fits will have little or no relation to any meaningful atmospheric property. All of the quantitative expressions stated in this work concerning the relationships between ionospheric electron densities, solar flux, and SZA angle are invalid if a profile does not have an alpha-Chapman shape.

Do these unusual shapes mean that the data from Period 4 is incorrect or of poor quality? The mean peak electron density in Period 4, $7 \times 10^4\,\text{cm}^{-3}$, is very similar to the mean peak electron densities in the other Periods. The measurement errors in Period 4, typically $6 \times 10^3\,\text{cm}^{-3}$, are about 50% larger than those from the other Periods, but are not large enough to invalidate use of the data.

Scale heights derived for profiles in Periods 1–3 do not show much variation. If we assume a constant value of H for all the profiles in Period 4 and produce plots analogous to those of Fig. 6, then we actually see the opposite of the predicted correlation curve; a trough in the correlation curve is seen at an offset of zero days instead of a peak. Our earlier results for Periods 1–3 are not significantly altered if we assume a constant value of H.

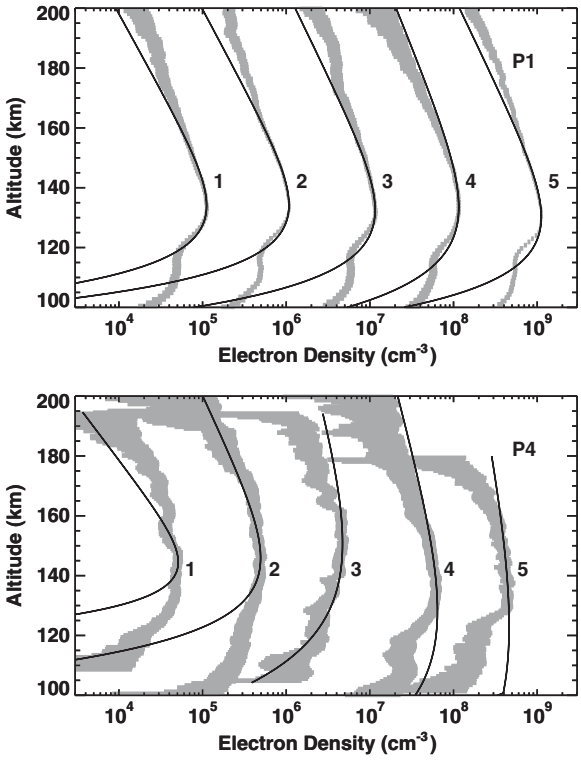

Fig. 7. The top panel shows five electron density profiles and their 1σ uncertainties from Period 1. The uncertainties are marked by the shaded region and the nominal profiles, which are not marked by any line, are at the centers of those regions. An alpha-Chapman fit to each profile, calculated as discussed in Section 2.1, is also plotted as a solid line. In all five cases, the fit and the data disagree slightly at high altitudes, agree well around the "M2" peak, and disagree significantly around the "M1" peak. This is consistent with the discussion in Section 1.4 and is also similar to results (not shown) for Periods 2 and 3. The profile labelled "1" is 1100I41A.EDS, "2" is 1105I24A.EDS, "3" is 1089F46A.EDS, "4" is 1092S10A.EDS, and "5" is 1096Q22A.EDS. For display purposes, the electron densities in the first profile (numbered 1) have been multiplied by a factor of 1, those in the second profile have been multiplied by a factor of 10, and so on, with those in the last and fifth profile having been multiplied by a factor of 10^4. The bottom panel is similar to the top panel, but shows profiles from Period 4. Unlike Period 1, the fits and the data for Period 4 disagree significantly in many respects. The profile labelled "1" is 9128P56A.EDS, "2" is 9126Q52A.EDS, "3" is 9128M00A.EDS, "4" is 9132I11A.EDS, and "5" is 9126M56A.EDS.

4.4. Discussion of unexpected results from Period 4

Why is Period 4 so different from the other three? As Table 1 shows, its range of SZAs is comparable to that of Period 3 and its Ls is very similar to that of Period 1. It, like Period 3, is near opposition. It is not a nightside ionosphere because (a) the electron densities are much too high (Fox et al., 1993; Zhang et al., 1990; McCormick and Whitten, 1990) and (b) its measurements are made many photochemical time constants after sunrise. As discussed in Martinis et al. (2003), photochemical time constants, τ_{PC}, satisfy $\tau_{PC} \alpha N = 1$.

Since $\alpha = 2 \times 10^{-7}\,\mathrm{cm^3\,s^{-1}}$ and $N_m \sim 7 \times 10^4\,\mathrm{cm^{-3}}$, $\tau_{PC} \sim 1$ min.

Measurements for Periods 1–3 were made at northern latitudes during spring/summer, whereas measurements for Period 4 were made at southern latitudes during winter. General circulation models predict that the composition and dynamics of the neutral atmosphere will vary between seasons and between hemispheres (Bougher et al., 2000). Wind speeds greater than $300\,\mathrm{m\,s^{-1}}$ have been predicted at 200 km altitude for the latitude, LST, and Ls of Period 4, which correspond to the boundary of the vortex that dynamically isolates the dark winter pole from the rest of the atmosphere. Atmospheric dynamics can disturb the ionosphere directly. Indirectly, they can cause compositional variations in the neutral atmosphere that alter the ionosphere. Large dynamical effects of a spatial scale smaller than the model resolution, such as gravity waves, could also be important. These effects are not restricted in longitude.

Period 4 is the only one with measurements at southern latitudes over the crustal magnetic fields there (Purucker et al., 2000; Acuña et al., 2001; Connerney et al., 2001). The presence of magnetic fields can affect an ionosphere in several ways, as discussed in Hargreaves (1992) and Rishbeth and Garriott (1969). Firstly, they can modify the influx of energetic particles from the solar wind and outflow of hot ions, which affects the thermal structure of the neutral atmosphere. Secondly, they can alter the direction of ambipolar plasma diffusion from the vertical. However, ion diffusion in any direction is not expected to be significant at the low altitudes of the primary ionospheric peak. Thirdly, they can alter the original horizontal direction of ion transport by horizontal winds. Timescales for this process are $\sim H/u$, where u is the horizontal wind speed. Using $H = 10$ km and $u = 100\,\mathrm{m\,s^{-1}}$ gives a timescale of 100 s, comparable to the photochemical timescale, τ_{PC} (Bougher et al., 1990). Krymskii et al. (2003) and Breus et al. (2004) suggest that electron temperatures in the ionosphere are greater in the southern hemisphere than in the northern hemisphere due to the presence of large magnetic anomalies in the southern hemisphere. Observed effects of the crustal magnetic anomalies on the ionosphere are also discussed by Ness et al. (2000), Mitchell et al. (2001), Krymskii et al. (2002), and Withers et al. (2005).

The crustal magnetic anomalies are not uniformly distributed in longitude (Connerney et al., 2001, 2004). In the 64–69°S latitude range of the Period 4 data, strong magnetic fields are only found for longitudes greater than 90°E and less than 270°E. Many, but not all, electron density profiles with longitudes within this range have unusual shapes. A significant number of electron density profiles from outside this longitude range also have unusual shapes, despite being outside the region of strong crustal magnetic anomalies. We can repeat our correlation analysis, assuming a constant scale height, for Period 4 with two subsets of data corresponding to these two longitude regions. The results are shown in Fig. 8. In the region of strong magnetic fields, Q increases as time passes. In the region of weak magnetic fields, Q appears scattered about a constant value and shows no trend with time. Since Period 4 is near opposition, $E_{10.7}^{\mathrm{Mars,1\,AU}}$ values should be nearly identical to the known $E_{10.7}^{\mathrm{Earth,1\,AU}}$ values. Neither of these two subsets of data shows Q increasing as $E_{10.7}^{\mathrm{Mars,1\,AU}}$ increases nor Q decreasing as $E_{10.7}^{\mathrm{Mars,1\,AU}}$ decreases, although the uncertainties on the correlation curve for the region of weak magnetic fields are rather large.

One additional complication is the occultation geometry involved in the ionospheric measurements (Ness et al., 2000). The actual phase shift measurement that is made during an occultation includes contributions from a horizontally extended region within the ionosphere, but it is referenced to a single horizontal position after processing. As an example, a measurement nominally made at an altitude of z has a ray path with a closest approach to the planet of z. This ray path crosses the altitude $z + H$ a horizontal distance $\sqrt{2HR}$ away from this closest approach point. This horizontal distance is on the order of a few hundred kilometers. This might cause the ionosphere within the regions of strong magnetic fields to influence the measured, but not actual, electron density outside these regions.

If we examine the ionospheric dependence on SZA for Period 4, using the techniques of Section 2.1 and a constant scale height of 12 km, then both subsets of Period 4 data, when plotted as in Fig. 2, have best fits similar to Eq. (6). Krymskii et al. (2003) also showed that the dependence of N_m on χ for Period 4 was consistent with the Chapman prediction that $N_m \propto (Ch)^{-1/2}$. Bougher et al. (2004) showed that the peak altitude for the Period 4 data, z_m, is consistent with the Chapman prediction that $z_m = z_0 + H \ln Ch$. Some features of the Period 4 data are clearly consistent with Chapman theory, suggesting that the data quality is acceptable, even if the profile shapes are not.

4.5. The martian ionosphere as a monitor of farside solar activity

Our two hypotheses have an interesting and useful corollary: Q, which can be derived from routine ionospheric observations, can be converted into $E_{10.7}^{\mathrm{Mars,1\,AU}}$, thus providing a monitor of solar activity from a second vantage point in the solar system. It has long been an aim of the solar-terrestrial science community to observe the farside of the Sun. Fig. 9 shows the relationship between Q and $E_{10.7}^{\mathrm{Mars,1\,AU}}$ using data from Period 1,

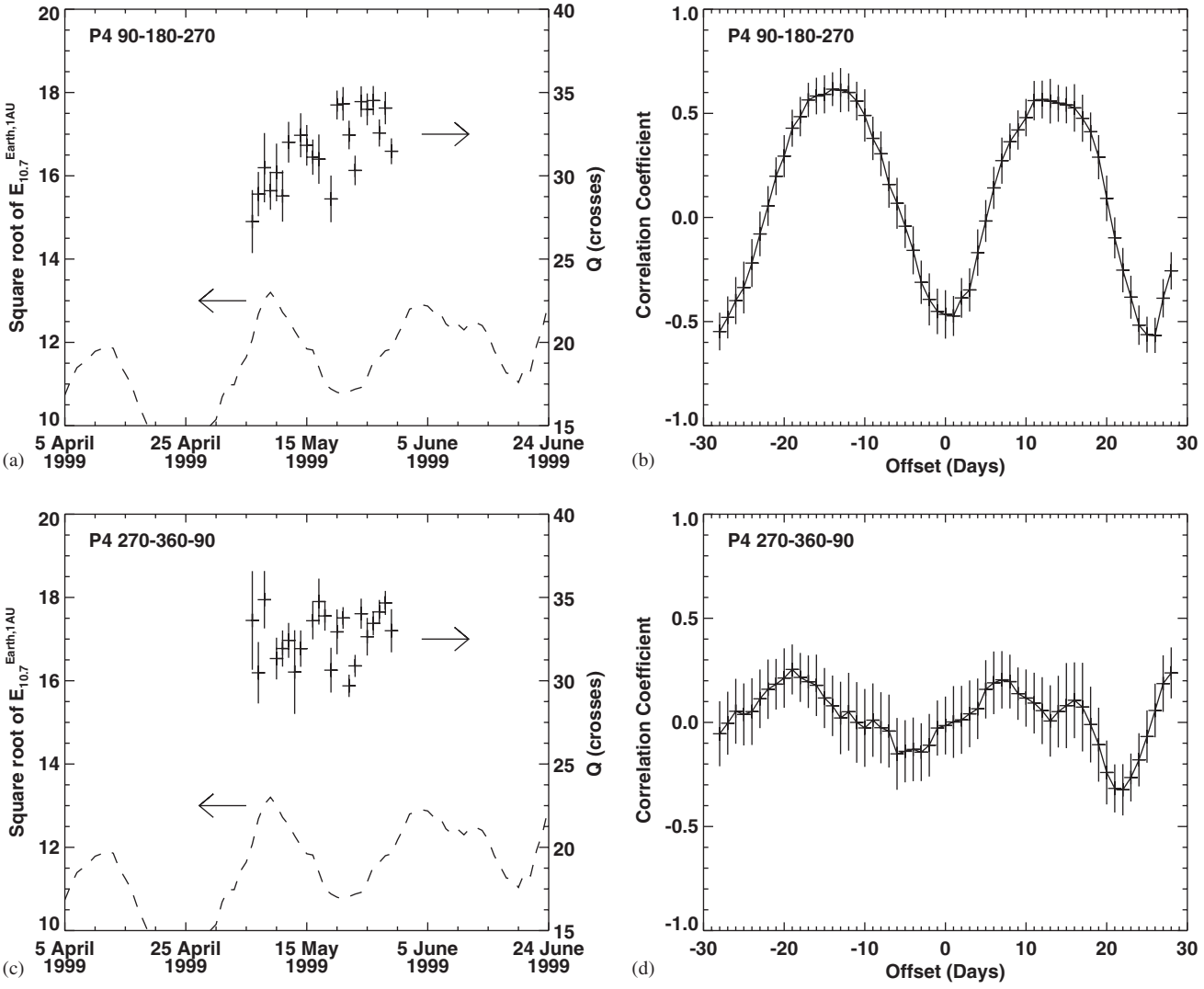

Fig. 8. This figure is similar to Fig. 6, except that it displays two subsets of data from Period 4 instead of data from Periods 1–3. The top row displays data from 109 vertical electron density profiles with longitudes greater than 90°E and less than 270°E. The bottom row displays data from 111 vertical electron density profiles with longitudes less than 90°E or greater than 270°E.

which had the best correlation between ionospheric response and solar stimulus. The best fit line is

$$\ln((N_m/10^4\,\mathrm{cm}^{-3})\sqrt{H/10\,\mathrm{km}\,Ch}\,(D/\mathrm{AU})) = (0.243 \pm 0.031)\ln(E_{10.7}^{\mathrm{Mars,1\,AU}}) + (2.181 \pm 0.165). \quad (11)$$

Note that this fit uses $E_{10.7}^{\mathrm{Mars,1\,AU}}$, not $E_{10.7}^{\mathrm{Earth,1\,AU}}$. We have timeshifted $E_{10.7}^{\mathrm{Earth,1\,AU}}$ by the predicted offset (see Table 1) to obtain $E_{10.7}^{\mathrm{Mars,1\,AU}}$. This fit does not change significantly if we set H to a constant value of 12 km. We will discuss the implications of the derived gradient, 0.243 ± 0.035, in Section 5.2. Studies of the time history of proxies for solar flux at Earth have given scientists rich insights into the dynamic behavior of the outermost regions of the Sun, and stars in general. Knowledge of the Sun's flux at another location within the Solar

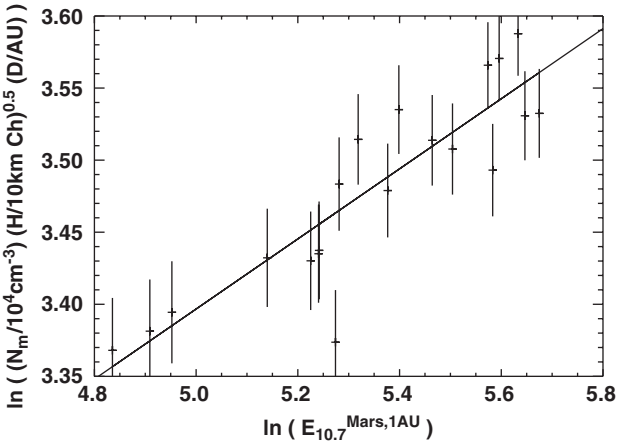

Fig. 9. Dependence of daily averages of $Q = N_m/(10^4\,\mathrm{cm}^{-3})\sqrt{H/(10\,\mathrm{km})Ch}(D/\mathrm{AU})$ on solar flux for Period 1. The vertical lines are $\pm 1\sigma$ error bars. A best fit line, Eq. (11), is also shown.

System, as provided by martian ionospheric observations, will help solar physicists develop a more accurate understanding of our Sun.

5. Discussion

5.1. What have we accomplished?

In Section 2, we related peak electron density in the martian ionosphere to SZA using simple Chapman theory and assuming constant solar flux. The constant solar flux derived from this relationship is consistent with the Solar2000 model's characterization of solar flux. In Section 3, we demonstrated that residuals between our observations and a theoretical fit were due to changes in solar flux. We qualitatively found that the occurrence of these residuals was controlled by the Earth–Sun–Mars angle and solar rotation period, indicating a delayed response on Mars to solar changes observed from Earth as the active regions on the Sun rotate from facing Earth to face Mars. In Section 4, we quantitatively demonstrated in three separate cases that the martian ionosphere responds to changes in solar flux *as measured at Earth* with lead/lag times that are consistent with independent measurements of the solar rotation period. This solar rotation-controlled response only occurs when day-to-day changes in solar flux at Mars are due to solar rotation and not to temporal growth or decay of solar active regions. The correlation between changes in the ionosphere and changes in solar flux is strongest when solar flux is greatest and/or the change in solar flux is greatest. Electron density profiles from the southern hemisphere do not have the alpha-Chapman shape predicted by theory and observed in the northern hemisphere. Their peak electron densities are not controlled as consistently by the flux of ionizing ultraviolet and X-ray radiation from the Sun as is seen in three datasets from the northern hemisphere. This is true at *all* longitudes, though it is most evident in the 90–270°E region of strong crustal magnetic anomalies.

5.2. Comparison of ionospheric responses to short-term and long-term variations in solar flux

Several other workers have investigated ionospheric response to $F_{10.7}$ or $E_{10.7}$. Since we regard the changes in these proxies due to changes in heliocentric latitude and longitude and due to distance from the Sun as important, we will modify their published relationships by adding superscripts to these proxies to indicate their procedure. A subscript of "Mars" will generally indicate values derived by timeshifting from measurements at Earth.

Hantsch and Bauer (1990) have shown that $\mathrm{d}\ln N_m/\mathrm{d}\ln F_{10.7}^{\mathrm{Earth,1\,AU}} = 0.36$, without any error bars, for year-to-year changes in solar flux, where they adjusted observed N_m to zenith by dividing observed values by the square root of $\cos(\chi)$. Breus et al. (2004) have shown that $\mathrm{d}\ln(N_m\sqrt{H\sec\chi})/\mathrm{d}\ln E_{10.7}^{\mathrm{Mars,1\,AU}} = 0.37 \pm 0.06$ for changes in solar flux over a few months. Note that they used $\sec(\chi)$ as an approximation for Ch. Our Section 4.5 results for a 20 day interval have $\mathrm{d}\ln(N_m\sqrt{H\,Ch})/\mathrm{d}\ln E_{10.7}^{\mathrm{Mars,1\,AU}} = 0.243 \pm 0.031$. Stewart and Hanson (1982) did not calculate a best fit value for $\mathrm{d}\ln(N_mD)/\mathrm{d}\ln F_{10.7}$, but stated that a value of 0.5 could be used in a model which fitted observed N_m from all missions up to and including Viking with a root-mean-square deviation of about 10%. Why are our results different from those of previous workers?

If we analyze the November 2000–January 2001 period investigated by Breus et al. (2004) using the methods of this paper, we obtain $\mathrm{d}\ln(N_m\sqrt{H\,Ch})/\mathrm{d}\ln E_{10.7}^{\mathrm{Mars,1\,AU}} = 0.191 \pm 0.035$. Breus et al. (2004) used version 1.24 of Solar2000, whereas we have used version 2.23. If we use version 1.24 of Solar2000 to obtain $E_{10.7}^{\mathrm{Mars,1\,AU}}$ values, then we obtain $\mathrm{d}\ln(N_m\sqrt{H\,Ch})/\mathrm{d}\ln E_{10.7}^{\mathrm{Mars,1\,AU}} = 0.275 \pm 0.046$. If we also replace Ch with $\sec(\chi)$, then we obtain a value of 0.318 ± 0.046. It is likely that Breus et al. (2004) used only a partial subset of their November 2000–January 2001 data in their fit to exclude any SZAs that exceeded some threshold (Kymskii, 2005, personal communication). The difference between our result and that of Breus et al. (2004) is mainly due to changes in Solar2000, differences between Ch and $\sec\chi$, and their unknown SZA constraints. The remaining difference can be attributed to different procedures for finding N_m, H, and their uncertainties. Returning to our Period 1, we find $\mathrm{d}\ln(N_m\sqrt{H\,Ch})/\mathrm{d}\ln E_{10.7}^{\mathrm{Mars,1\,AU}} = 0.290 \pm 0.037$ if we use version 1.24 of Solar2000.

For comparison with Hantsch and Bauer (1990), we found that $\mathrm{d}\ln(N_m\sqrt{\sec(\chi)})/\mathrm{d}\ln F_{10.7}^{\mathrm{Mars,1\,AU}} = 0.242 \pm 0.012$ for Period 1. Our results might be biased because we have a small range in $\ln(F_{10.7}^{\mathrm{Mars,1\,AU}})$, which makes them quite sensitive to any minor changes in the fitted data. The results of Hantsch and Bauer (1990) may be biased because they did not correct for changes in Mars–Sun distance, used $\sec(\chi)$ as an approximation for Ch despite having some data at SZAs over 85°, did not account for differences between $F_{10.7}^{\mathrm{Mars,1\,AU}}$ and $F_{10.7}^{\mathrm{Earth,1\,AU}}$, and treated individual ionospheric measurements from flyby spacecraft, such as Mars 2, on equal terms with the averages of many measurements from orbiting spacecraft, such as Mariner 9. The majority of their data points have $100 < F_{10.7}^{\mathrm{Earth,1\,AU}} < 150$ and solar rotation can easily cause $F_{10.7}^{\mathrm{Earth,1\,AU}}$ to differ from $F_{10.7}^{\mathrm{Mars,1\,AU}}$ by 50 flux units.

Our 20-day Period 1 is not extensive enough to justify the use of Eq. (11) without consideration and acknowledgement of the slightly different results obtained by other workers using other datasets, assumptions, and techniques. One unusual feature of our Period 1, compared with the datasets of other workers, is that χ only spans 71.8°–72.8°. Nevertheless, it does offer some advantages over the pre-MGS work of Hantsch and Bauer (1990). Given that photochemical timescales at the daytime ionospheric peak are on the order of a minute, we do not expect that the day-to-day response of the martian ionosphere to changes in solar flux differs from its response to year-to-year changes. However, there could be year-to-year changes in the neutral atmosphere, within which the ionosphere is embedded, and there are probably Sun–atmosphere–ionosphere couplings on these longer timescales that are in need of further study.

5.3. Mars and Venus

Since the main atmospheric neutral, CO_2, and the main ion, O_2^+, are the same on both Mars and Venus, it is instructive to compare their respective responses to changes in solar flux. Bauer and Hantsch (1989) fitted alpha-Chapman shapes to electron density profiles on Venus and Mars and derived neutral scale heights, H. They found that $H \propto (F_{10.7}^{\text{Earth,1 AU}})^m$ where m is 0.14 and 0.16 for Venus and Mars, respectively. They did not state any error bars on these derived exponents.

For the ionosphere of Venus, best fits to the power law $N_m \propto (F_{10.7}^{\text{Venus,0.72 AU}})^m$ over periods comparable to a solar cycle found that m is 0.376 ± 0.011 (Kliore and Mullen, 1989). For the ionosphere of Mars, best fits to the power law $N_m \propto (F_{10.7}^{\text{Earth,1 AU}})^m$ over periods comparable to a solar cycle found that m is 0.36 (Hantsch and Bauer, 1990). Since Venus does not have an eccentric orbit, but Mars does, the result for Mars may be less reliable than that for Venus.

Mitchell et al. (2000) have also investigated the influence of solar rotation in the topside martian ionosphere. They found that MGS Electron Reflectometer observations of the flux of oxygen Auger electrons at 170 km altitude near solar conjunction were correlated with solar X-ray fluxes measured at Earth during April 1998 if the X-ray fluxes were timeshifted to compensate for solar rotation. They tested a range of possible solar rotation periods and found a good correlation only for timeshifts using periods of 25–28 days.

Elphic et al. (1984) examined how electron densities in the ionosphere of Venus varied in response to short-term variations in a solar flux proxy measured at Venus. Their solar flux proxy is not particularly representative, and their correlation was quite weak, but they obtained a best fit power law with an exponent of 0.33 (Fox and Kliore, 1997). Considering those caveats, their result is consistent with the 0.376 ± 0.011 exponent of Kliore and Mullen (1989).

These many similarities between Mars and Venus lead us to support the assumption of Kliore and Mullen (1989) that the ionosphere of Venus should also respond to changes in solar flux *as measured at Earth* with lead/lag times that are consistent with independent measurements of the solar rotation period. A test of this assumption would be useful.

5.4. Response of the terrestrial ionosphere to changes in solar flux

As discussed by Mendillo et al. (2003), the region of the terrestrial ionosphere that is most similar to the main ionospheric layers of Mars and Venus is the E-region, which is dominated by photochemistry, rather than transport, and molecular, rather than atomic, ions. Titheridge (1997) suggested a parameterization for the dependence of N_mE, the maximum electron density within the E region, on $F_{10.7}$ based upon the experimentally based International Reference Ionosphere. Following Titheridge's discussion of the optimum parameterization, we set B, the $F_{10.7}$ offset term, equal to 40 in his Eq. (12). We find that $\mathrm{d}\ln N_mE/\mathrm{d}\ln F_{10.7}$ increases monotonically as $F_{10.7}$ increases, having a value of 0.32 at $F_{10.7} = 70$ and 0.43 at $F_{10.7} = 250$. Rishbeth and Garriott (1969) suggest a parameterization for N_mE in terms of sunspot number. Sunspot number is well correlated with $F_{10.7}$. We use Rishbeth and Garriott's Equation 504 and a relationship between sunspot number and $F_{10.7}$ from Sello (2003) to calculate $\mathrm{d}\ln N_mE/\mathrm{d}\ln F_{10.7}$. In this case, $\mathrm{d}\ln N_mE/\mathrm{d}\ln F_{10.7}$ does not change monotonically with $F_{10.7}$, but varies between about 0.35 and 0.50. Hargreaves (1992) also suggests a slightly different parameterization for N_mE in terms of sunspot number in his Eq. (7.5). In this case, $\mathrm{d}\ln N_mE/\mathrm{d}\ln F_{10.7}$ does not change monotonically with $F_{10.7}$, but varies between about 0.30 and 0.45. Despite the many differences between the terrestrial E-region and the ionospheres of Mars and Venus, all three seem fairly well-described by $\mathrm{d}\ln N_m/\mathrm{d}\ln E_{10.7}$ or $\mathrm{d}\ln N_m/\mathrm{d}\ln F_{10.7} \sim 0.35-0.40$ when corrections for Sun-planet distance and solar rotation are applied to the solar flux proxy. A common factor in these three ionospheric regions is the importance of dissociative recombination of O_2^+ ions for ion loss, whose rate appears as α in Eq. (1), and its dependence upon electron temperature.

5.5. Future observations

Mars is a current focus of planetary exploration, so we can expect continued ionospheric observations by radio occultations using other spacecraft after MGS

eventually ceases operations. A crucial need is coverage at local times away from the dawn and dusk sectors, which could be provided by satellite-to-satellite occultation measurements or, of course, by surface-to-satellite radio systems, as used with the terrestrial GPS network (Mendillo et al., 2004). Ionospheric observations at a wide range of latitudes should be obtained from by Mars Express from limb occultations from its radio science experiment and nadir topside sounding from its radar. These observations will be complemented by simultaneous measurements of the neutral atmosphere on Mars Express that provide a context for interpreting the ionospheric data.

Large numbers of ionospheric measurements spanning the full range of solar activity over a solar cycle, which are needed to characterize the dependence of the mean state and variability of the martian ionosphere on solar flux, should be available once the MGS and Mars Express missions are completed. Simultaneous measurements of solar flux, the ionosphere, and the neutral atmosphere are still needed to unravel the detailed interactions of this coupled system.

In addition to providing a more complete picture of our dynamic and changing Sun, as discussed in Section 4.5, Mars-based observations of solar activity could provide a warning of any intense solar activity about to rotate to impact the Earth's environment. However, this would only be useful within a limited range of Earth–Sun–Mars angles, would require fast, operational data processing rather than the current slower, science-driven data processing, and would only be sensitive to solar photons and not to the more damaging solar-emitted particles.

Bougher et al. (2004) have suggested monitoring the ionospheric peak altitude as a way of monitoring thermospheric dynamics. This is complementary to our suggestion of studying the ionospheric peak magnitude to monitor solar activity.

Acknowledgements

We gratefully acknowledge many enlightening discussions with Dave Hinson, and his continuing efforts in processing this rich dataset and making it publicly available. We acknowledge the work of the referee. This work was supported, in part, by NASA's Mars Data Analysis Program (NNG04GK76G), by the NSF CEDAR program (ATM-0334383), and by seed research funds from the Center for Space Physics at Boston University. PW acknowledges support from Arden Albee and the Sixth International Mars Conference. SOLAR2000 Research Grade historical irradiances are provided courtesy of W. Kent Tobiska and SpaceWx.com. These historical irradiances have been developed with funding from the NASA UARS, TIMED, and SOHO missions.

References

Acuña, M.H., Connerney, J.E.P., Wasilewski, P.J., Lin, R.P., Mitchell, D.L., Anderson, K.A., Carlson, C.W., McFadden, J., Reme, H., Mazelle, C., Vignes, D., Bauer, S.J., Cloutier, P., Ness, N.F., 2001. Magnetic field of Mars: summary of results from the aerobraking and mapping orbits. J. Geophys. Res. 106 (E10), 23,403–23,418.

Barth, C.A., Hord, C.W., Pearce, J.B., Kelly, K.K., Anderson, G.P., Stewart, A.I.F., 1971. Mariner 6 and 7 ultraviolet spectrometer experiment: upper atmospheric data. J. Geophys. Res. 76, 2213–2227.

Barth, C.A., Stewart, A.I.F., Hord, C.W., Lane, A.L., 1972. Mariner 9 ultraviolet spectrometer experiment: Mars airglow spectroscopy and variations in Lyman alpha. Icarus 17, 457–468.

Barth, C.A., Stewart, A.I.F., Bougher, S.W., Hunten, D.M., Bauer, S.J., Nagy, A.F., 1992. Aeronomy of the current martian atmosphere. In: Kieffer, H.H., Jakosky, B.M., Snyder, C.W., Matthews, M.S. (Eds.), Mars. University of Arizona Press, Arizona, pp. 1054–1089.

Bauer, S.J., Hantsch, M.H., 1989. Solar cycle variation of the upper atmosphere temperature of Mars. Geophys. Res. Lett. 16 (5), 373–376.

Bevington, P.R., 1969. Data Reduction and Error Analysis for the Physical Sciences, 1st ed. McGraw-Hill, New York.

Bougher, S.W., Roble, R.G., Ridley, E.C., Dickinson, R.E., 1990. The Mars thermosphere. II—general circulation with coupled dynamics and composition. J. Geophys. Res. 95 (B9), 14,811–14,827.

Bougher, S.W., Engel, S., Roble, R.G., Foster, B., 2000. Comparative terrestrial planet thermospheres 3. Solar cycle variation of global structure and winds at solstices. J. Geophys. Res. 105 (E7), 17,669–17,692.

Bougher, S.W., Engel, S., Hinson, D.P., Forbes, J.M., 2001. Mars Global Surveyor Radio Science electron density profiles: neutral atmosphere implications. Geophys. Res. Lett. 28 (16), 3091–3094.

Bougher, S.W., Engel, S., Hinson, D.P., Murphy, J.R., 2004. MGS Radio Science electron density profiles: interannual variability and implications for the martian neutral atmosphere. J. Geophys. Res. 109, E03010, doi:10.1029/2003JE002154.

Breus, T.K., Krymskii, A.M., Crider, D.H., Ness, N.F., Hinson, D., Barashyan. K.K., 2004. Effect of the solar radiation in the topside atmosphere/ionosphere of Mars: Mars Global Surveyor observations. J. Geophys. Res. (Space Phys.) 109 (A18), doi:10.1029/2003JE002154.

Chamberlain, J.W., Hunten, D.M., 1987. Theory of Planetary Atmospheres. 2nd ed. Academic Press, New York.

Chapman, S., 1931a. The absorption and dissociative or ionizing effect of monochromatic radiation in an atmosphere on a rotating Earth. Proc. Phys. Soc. 43, 26–45.

Chapman, S., 1931b. The absorption and dissociative or ionizing effect of monochromatic radiation in an atmosphere on a rotating Earth. Part II. Grazing incidence. Proc. Phys. Soc. 43, 483–501.

Chen, R.H., Cravens, T.E., Nagy, A.F., 1978. The martian ionosphere in light of the Viking observations. J. Geophys. Res. 83 (A8), 3871–3876.

Connerney, J.E.P., Acuña, M.H., Wasilewski, P.J., Kletetschka, G., Ness, N.F., Reme, H., Lin, R.P., Mitchell, D.L., 2001. The global magnetic field of Mars and implications for crustal evolution. Geophys. Res. Lett. 28 (21), 4015–4018.

Connerney, J.E.P., Acuña, M.H., Ness, N.F., Mitchell, D.L., Lin, R.P., 2004. An extraordinary magnetic field map of Mars. Lunar and Planetary Science Conference, vol. 35. Abstract #1114.

Elphic, R.C., Brace, L.H., Theis, R.F., Russell, C.T., 1984. Venus dayside ionosphere conditions: effects of ionospheric magnetic field and solar EUV flux. Geophys. Res. Lett. 11 (2), 124–127.

Fox, J.L., 1993. The production and escape of nitrogen atoms on Mars. J. Geophys. Res. 98 (E2), 3297–3310.

Fox, J.L., 2004a. Advances in the aeronomy of Venus and Mars. Adv. Space Res. 33 (2), 132–139.

Fox, J.L., 2004b. Response of the Martian thermosphere/ionosphere to enhanced fluxes of solar soft X rays. J. Geophys. Res. (Space Phys.) 109 (A18), doi:10.1029/2004JA010380.

Fox, J.L., Kliore, A.J., 1997. Ionosphere: solar cycle variations. In: Bougher, S.W., Hunten, D.M., Phillips, R.J. (Eds.), Venus II. University of Arizona Press, Arizona, pp. 161–188.

Fox, J.L., Brannon, J.F., Porter, H.S., 1993. Upper limits to the nightside ionosphere of Mars. Geophys. Res. Lett. 20 (13), 1339–1342.

Fox, J.L., Zhou, P., Bougher, S.W., 1996. The martian thermosphere/ionosphere at high and low solar activities. Adv. Space Res. 17 (11), 203–218.

Haider, S.A., Seth, S.P., Kallio, E., Oyama, K.I., 2002. Solar EUV and electron–proton–hydrogen atom-produced ionosphere on Mars: comparative studies of particle fluxes and ion production rates due to different processes. Icarus 159, 18–30.

Hanson, W.B., Sanatani, S., Zuccaro, D.R., 1977. The martian ionosphere as observed by the Viking retarding potential analyzers. J. Geophys. Res. 82, 4351–4363.

Hantsch, M.H., Bauer, S.J., 1990. Solar control of the Mars ionosphere. Planet. Space Sci. 38 (4), 539–542.

Hargreaves, J.K., 1992. The Solar-terrestrial Environment. Cambridge University Press, New York.

Hinson, D.P., Simpson, R.A., Twicken, J.D., Tyler, G.L., Flasar, F.M., 1999. Initial results from radio occultation measurements with Mars Global Surveyor. J. Geophys. Res. 104 (E11), 26,997–27,012.

Hinson, D.P., Simpson, R.A., Twicken, J.D., Tyler, G.L., Flasar, F.M., 2000. Erratum: initial results from radio occultation measurements with Mars Global Surveyor. J. Geophys. Res. 105 (E1), 1717–1718.

Kallio, E., Janhunen, P., 2001. Atmospheric effects of proton precipitation in the martian atmosphere and its connection to the Mars-solar wind interaction. J. Geophys. Res. 106 (A4), 5617–5634.

Kliore, A.J., 1992. Radio occultation observations of the ionospheres of Mars and Venus. In: Luhmann, J.G., Tatrallyay, M., Pepin, R.O. (Eds.), Venus and Mars: Atmospheres, Ionospheres, and Solar Wind Interactions, Geophysical Monograph Series, vol. 66. AGU, Washington DC, pp. 265–276.

Kliore, A.J., Mullen, L.F., 1989. The long-term behavior of the main peak of the dayside ionosphere of Venus during solar cycle 21 and its implications on the effect of the solar cycle upon the electron temperature in the main peak region. J. Geophys. Res. 94 (A10), 13,339–13,351.

Krasnopolsky, V.A., 2002. Mars' upper atmosphere and ionosphere at low, medium, and high solar activities: implications for evolution of water. J. Geophys. Res. 107 (E12), 5128, doi:10.1029/2001JE001809.

Krymskii, A.M., Breus, T.K., Ness, N.F., Acuña, M.H., Connerney, J.E.P., Crider, D.H., Mitchell, D.L., Bauer, S.J., 2002. Structure of the magnetic field fluxes connected with crustal magnetization and topside ionosphere at Mars. J. Geophys. Res. 107 (A9), 1245, doi:10.1029/2001JA000239.

Krymskii, A.M., Breus, T.K., Ness, N.F., Hinson, D.P., Bojkov, D.I., 2003. Effect of crustal magnetic fields on the near terminator ionosphere at Mars: comparison of in situ magnetic field measurements with the data of radio science experiments on board Mars Global Surveyor. J. Geophys. Res. 108 (A12), 1431, doi:10.1029/2002JA009662.

Krymskii, A.M., Ness, N.F., Crider, D.H., Breus, T.K., Acuña, M.H., Hinson, D.P., 2004. Solar wind interaction with the ionosphere/atmosphere and crustal magnetic fields at Mars: Mars Global Surveyor Magnetometer/Electron Reflectometer, radio science, and accelerometer data. J. Geophys. Res. (Space Phys.) 109 (A18), doi:10.1029/2004JA010420.

Martinis, C.R., Wilson, J.K., Mendillo, M.J., 2003. Modeling day-to-day ionospheric variability on Mars. J. Geophys. Res. 108 (A10), 1383, doi:10.1029/2003JA009973.

McCormick, P.T., Whitten, R.C., 1990. The dynamics of the ionosphere of Mars at large solar zenith angles. J. Geophys. Res. 95 (A5), 6263–6269.

Mendillo, M., Smith, S., Wroten, J., Rishbeth, H., Hinson, D.P., 2003. Simultaneous ionospheric variability on Earth and Mars. J. Geophys. Res. 108 (A12), 1432, doi:10.1029/2003JA009961.

Mendillo, M.J., Pi, X., Smith, S., Martinis, C.R., Wilson, J.K., Hinson, D.P., 2004. Ionospheric effects upon a satellite navigation system at Mars. Radio Sci. 39, RS2028, doi:10.1029/2003RS002933.

Mitchell, D.L., Lin, R.P., Reme, H., Crider, D.H., Cloutier, P.A., Connerney, J.E.P., Acuña, M.H., Ness, N.F., 2000. Oxygen Auger electrons observed in Mars' ionosphere. Geophys. Res. Lett. 27 (13), 1871–1874.

Mitchell, D.L., Lin, R.P., Mazelle, C., Reme, H., Cloutier, P.A., Connerney, J.E.P., Acuña, M.H., Ness, N.F., 2001. Probing Mars' crustal magnetic field and ionosphere with the MGS Electron Reflectometer. J. Geophys. Res. 106 (E10), 23,419–23,427.

Molina-Cuberos, G.J., Witasse, O., Lebreton, J.-P., Rodrigo, R., Lopez-Moreno, J.J., 2003. Meteoric ions in the atmosphere of Mars. Planet. Space Sci. 51 (3), 239–249.

Ness, N.F., Acuña, M.H., Connerney, J.E.P., Kliore, A.J., Breus, T.K., Krymskii, A.M., Cloutier, P., Bauer, S.J., 2000. Effects of magnetic anomalies discovered at Mars on the structure of the martian ionosphere and solar wind interaction as follows from radio occultation experiments. J. Geophys. Res. 105 (A7), 15,991–16,004.

Nier, A.O., McElroy, M.B., 1977. Composition and structure of Mars' upper atmosphere—results from the neutral mass spectrometers on Viking 1 and 2. J. Geophys. Res. 82, 4341–4349.

Owen, T., 1992. The composition and early history of the atmosphere of Mars. In: Kieffer, H.H., Jakosky, B.M., Snyder, C.W., Matthews, M.S. (Eds.), Mars. University of Arizona Press, Arizona, pp. 818–834.

Press, W.H., Flannery, B.P., Teukolsky, S.A., Vetterling, W.T., 1992. Numerical Recipes in C: The Art of Scientific Computing. 2nd ed. Cambridge University Press, New York.

Purucker, M., Ravat, D., Frey, H., Voorhies, C., Sabaka, T., Acuña, M.H., 2000. An altitude-normalized magnetic map of Mars and its interpretation. Geophys. Res. Lett. 27 (16), 2449–2452.

Richards, P.G., 1994. EUVAC: a solar EUV flux model for aeronomic calculations. J. Geophys. Res. 99 (A5), 8981–8992.

Rishbeth, H., Garriott, O.K., 1969. Introduction to Ionospheric Physics. Academic Press, New York.

Rishbeth, H., Mendillo, M., 2004. Ionospheric layers of Earth and Mars. Planet. Space Sci. 52 (9), 849–852.

Schunk, R.W., Nagy, A.F., 2000. Ionospheres. Cambridge University Press, New York.

Sello, S., 2003. Solar cycle activity: a preliminary prediction for cycle #24. Astron. Astrophys. 410 (2), 691–693.

Shinagawa, H., 2004. The ionospheres of Venus and Mars. Adv. Space Res. 33 (11), 1924–1931.

Shinagawa, H., Bougher, S.W., 1999. A two-dimensional MHD model of the solar wind interaction with Mars. Earth Planets Space 51 (1), 55–60.

Shinagawa, H., Cravens, T.E., 1989. A one-dimensional multispecies magnetohydrodynamic model of the dayside ionosphere of Mars. J. Geophys. Res. 94 (A6), 6506–6516.

Smith III, F.L., Smith, C., 1972. Numerical evaluation of Chapman's grazing incidence integral. J. Geophys. Res. 77 (19), 3592–3597.

Stewart, A.I.F., 1972. Mariner 6 and 7 ultraviolet spectrometer experiment: implications of the CO_2^+, CO, and O airglow. J. Geophys. Res. 77, 54–68.

Stewart, A.I.F., Barth, C.A., Hord, C.W., Lane, A.L., 1972. Mariner 9 ultraviolet spectrometer experiment: structure of Mars' upper atmosphere. Icarus 17, 469–474.

Stewart, A.J., Hanson, W.B., 1982. Mars' upper atmosphere: mean and variations. Adv. Space Res. 2 (2), 87–101.

Titheridge, J.E., 1997. Model results for the ionospheric E region: solar and seasonal changes. Ann. Geophys. 15 (1), 63–78.

Tobiska, W.K., 2001. Validating the solar EUV proxy, E10.7. J. Geophys. Res. 106 (A12), 29,969–29,978.

Tobiska, W.K., Bouwer, S.D., 2004. New developments in the Solar2000 model for space research and operations. 35th COSPAR Scientific Assembly. Abstract #COSPAR04-A-00899.

Tobiska, W.K., Woods, T., Eparvier, F., Vierreck, R., Floyd, L., Bouwer, D., Rottman, G., White, O.R., 2000. The SOLAR2000 empirical solar irradiance model and forecast tool. J. Atmos. Solar-Terr. Phys. 62 (14), 1233–1250.

Tyler, G.L., Balmino, G., Hinson, D.P., Sjogren, W.L., Smith, D.E., Woo, R., Asmar, S.W., Connally, M.J., Hamilton, C.L., Simpson, R.A., 1992. Radio science investigations with Mars Observer. J. Geophys. Res. 97 (E5), 7759–7779.

Tyler, G.L., Balmino, G., Hinson, D.P., Sjogren, W.L., Smith, D.E., Simpson, R.A., Asmar, S.W., Priest, P., Twicken, J.D., 2001. Radio science observations with Mars Global Surveyor: orbit insertion through one Mars year in mapping orbit. J. Geophys. Res. 106 (E10), 23,327–23,348.

Wang, J.-S., Nielsen, E., 2003. Wavelike structures in the martian topside ionosphere observed by Mars Global Surveyor. J. Geophys. Res. 108 (E7), 5078, doi:10.1029/2003JE002078.

Wang, J.-S., Nielsen, E., 2004. Solar wind modulation of the martian ionosphere observed by Mars Global Surveyor. Ann. Geophys. 22 (6), 2277–2281.

Withers, P., Mendillo, M., Rishbeth, H., Hinson, D.P., Arkani-Hamed, J., 2005. Ionospheric characteristics above martian crustal magnetic anomalies. Geophys. Res. Lett. 32, L16204, doi:10.1029/2005GL023483.

Zhang, M.H.G., Luhmann, J.G., Kliore, A.J., 1990. An observational study of the nightside ionospheres of Mars and Venus with radio occultation methods. J. Geophys. Res. 95 (A10), 17,095–17,102.